Multiplexed Detection of Spike Patterns using Active Graphene Neurosensors

Carly V. Fengel*, Siyuan Yu†, Jinyong Kim†, Matthew L. Johnston†, and Ethan D. Minot*
*Department of Physics, Oregon State University, Corvallis, OR, 97331, USA
†School of Electrical Engineering and Computer Science, Oregon State University, Corvallis, OR, 97331, USA
Email: {fengelc, yusiy, kimjinyo, matthew.johnston, ethan.minot}@oregonstate.edu

2023 IEEE International Symposium on Circuits and Systems (ISCAS) | 978-1-6654-5109-3/23/$31.00 ©2023 IEEE | DOI: 10.1109/ISCAS46773.2023.10182074

***Abstract*—Traditional neurosensor arrays are constructed from passive metal electrodes that require one read-out wire for each sensor. The space required for wiring has become a critical bottleneck to increasing sensor count. It has been demonstrated that an array of active graphene sensors can be operated using less than one wire per sensor by using amplitude-modulation and frequency-division multiplexing (FDM), but results have been limited to measuring sub-kilohertz neural oscillations. In this work, we demonstrate an active graphene field effect transistor (GFET) electrode and FDM approach that can record spiking patterns with frequency components in the kilohertz band as required for single-neuron recordings, and combined sensor outputs on a single shared wire. Measured results include kilohertz signal bandwidth recovered from modulation frequencies up to 90 kHz, negligible cross-talk between signals transmitted on a shared output wire, and experiments showing that liquid-gated active graphene sensors can be operated with carrier frequencies up to 1 MHz. Long-term, megahertz carrier frequencies promise sufficient frequency-domain spacing to multiplex dozens of kilohertz neural signals on each shared output wire.**

***Index Terms*—Amplitude modulation, biosensors, frequency-division multiplexing, graphene**

I. Introduction

Electrical measurements of large populations of neurons can elucidate how information is processed in the brain. The need for such measurements is driving the development of neural probes that can record signals from thousands of sensors that are densely packed into a small area [1]. However, neural probes with high sensor count and high sensor density are challenging to connect to external electronics. Passive electrodes require a dedicated wire for every electrode, and active electrodes such as graphene transistors are typically operated with more than one wire per sensor [2]. These wires take up a large amount of space, limiting sensor density and total signal count. Moreover, there are practical limits on the number of wires that can be connected to recording hardware outside the brain. As such, this wiring bottleneck is a major obstacle to advancing neuroscience.

Multiplexing is a natural solution for decreasing wire count; for neurosensing applications, however, multiplexing is still in early development. One approach is to build active electrodes in which a miniaturized CMOS amplifier is located underneath every microelectrode site in the implanted probe [3]; in this case, the silicon integrated circuit (IC) must be carefully protected from salts in the physiological environment that degrade performance [4]. Moreover, this IC-based approach requires thick crystalline silicon substrates (thickness $\gg$50 μm), which makes the sensors mechanically rigid. The mechanical flexibility of neurosensors is a concern because long-term insertion of rigid probes into the soft tissue of the brain causes scarring, limiting long-term use and probe density [5], [6].

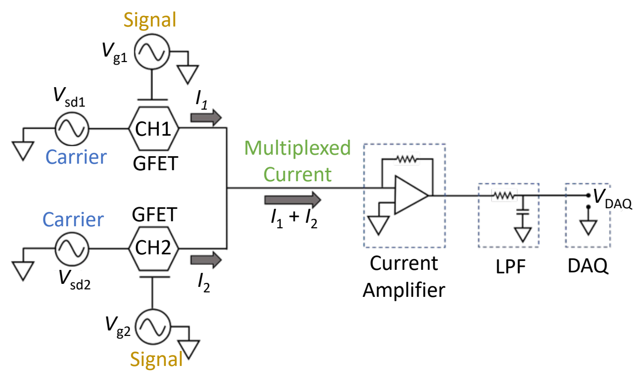

Fig. 1. Illustration of a 1×2 array of GFET neurosensors. The current output from each GFET is an amplitude-modulated (AM) current, and AM currents are summed on a single output wire.

In contrast, active graphene-based field effect transistor (GFET) sensors can be used to construct mechanically flexible neural probes with significantly reduced wire count, employing either time-division multiplexing [7] or frequency-division multiplexing (FDM) [8], although prior work is limited to sensing of neural activity at frequencies of 200 Hz or less. Concurrent work has explored ways to optimize IC-based readout designs for such multiplexed sensors [9]; in addition to reducing wire count, such approaches can reduce the number of needed analog-to-digital converters and readout hardware.

Graphene is an ideal transducer material for neurosensor applications because the resistance of a graphene transistor channel is sensitive to the local electrostatic environment, with signal-to-noise ratios comparable to passive metal electrodes [10], [11]. Changes in graphene resistance can be encoded in an amplitude-modulated (AM) current, which can be transmitted on a shared output wire, as shown in Fig. 1. Four additional properties contribute to graphene's unique potential: graphene has unprecedented mechanical flexibility [12], [13], graphene's electrical properties are not degraded by long-term exposure to physiological environments, healthy neuron growth on graphene suggests excellent biocompatibility [14]–[17], and graphene is optically transparent, therefore, simultaneous optical and electrical sensing is possible [18], [19].

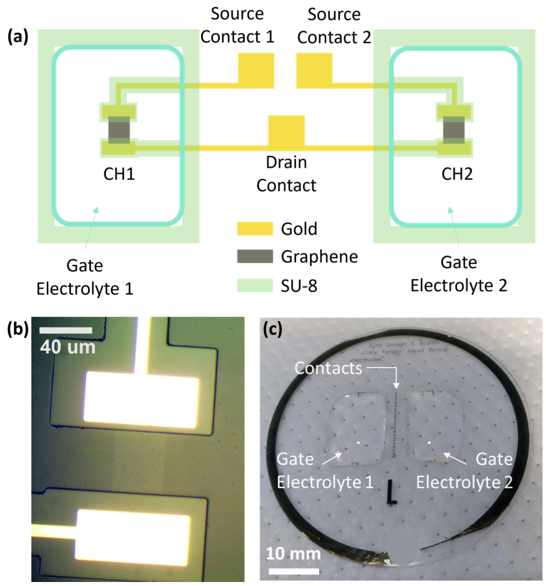

Fig. 2. Wafer design for multiplexing with two graphene FETs: (a) Illustration of one 1×2 array of GFETs. (b) Optical microscope image of a GFET; the graphene channel is visible in between the source and drain electrodes, electrodes and leads are passivated with SU-8. (c) Photograph of the 75 mm wafer with electrolyte in the two liquid gates.

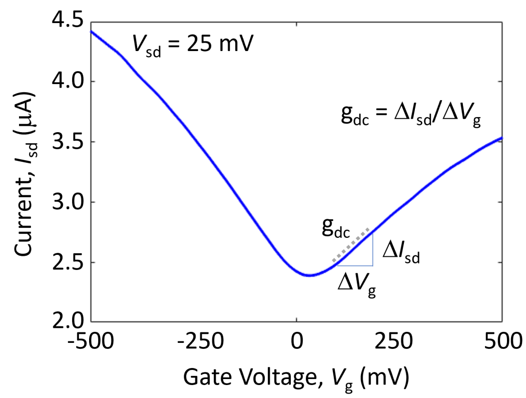

Fig. 3. Measured transfer characteristics of a GFET. The curve has been averaged over many cycles and smoothed with second-order LOESS smoothing.

In this work, we show that a GFET-based FDM detection scheme can record spiking patterns with frequency components in the kilohertz range. We further demonstrate a new dual-liquid-gate geometry for in-vitro testing mimicking independent neuron firing. We confirm that the modulation/demodulation process does not meaningfully degrade the signal-to-noise ratio of the sensor and demonstrate the absence of crosstalk between signals transmitted on a shared output wire. Lastly, we evaluate opportunities to scale the system by determining the frequency bands available for multiplexing.

II. Graphene Neurosensor Devices

A. Device Fabrication and Characterization

Prototype GFET active electrodes were fabricated on fused silica wafers. An illustration of one sensor pair is shown in Fig. 2a; Fig. 2b shows a microscope image of a single GFET device. The exposed channel dimensions are $W = L = 50\,\mu$m. A measured transfer curve for a GFET device is shown in Fig. 3. The wafer design consists of 23 pairs of GFETs that each share a common drain for collecting multiplexed current. While a 1×2 structure is used for testing, this is scalable to $1 \times N$ as limited by available bandwidth, as discussed in Sec. II-D. If a larger $N \times N$ array was used, N^2 sensors could be addressed with $2N$ wires, such that the number of wires would be substantially less than the number of sensors. The goal of this work is to first characterize properties of a small FDM-GFET array to inform the design of larger arrays.

Electrodes were defined using photolithography and deposited using electron beam evaporation (5 nm Cr, 40 nm Au). After metal lift-off, single-layer CVD-grown graphene (ACS Material) was added to the wafer via a wet transfer process [20]. Graphene was patterned using photolithography and oxygen plasma etch. After the graphene and electrodes were formed, the metal electrodes were encapsulated with a photopatterned layer of SU-8 polymer (SU-8 2002, Microchem). The SU-8 thickness was 1.4 μm. The SU-8 protects the source and drain leads from contacting the electrolyte, and forms hydrophobic rings to hold the two pools of electrolyte (Fig. 2).

B. Independent Liquid-Gate Measurement Setup

Each pair of GFET active electrodes in the array has two independent liquid gates. These gates were used to send independent signals to two GFET sensors, mimicking the action potentials of two independent, localized neurons. A pair of Ag/AgCl electrodes was used to apply the gate voltages to the two liquids. A signal generator (Rigol DG822) was used to control the gate signals and the dc offset of the gates. An additional signal generator applied the ac source-drain bias to each channel with an rms amplitude of 21 mV to act as the carrier (see Fig. 1). The multiplexed current was amplified with a low-noise current amplifier (Femto DLPCA-200) using a gain setting of 10^6 V/A and bandwidth of 500 kHz, and filtered through a custom anti-aliasing low-pass filter.

The analog current data was converted to a digital signal by a DAQ (National Instruments USB-6343) and saved for further processing. For most of the experiments described here, the data sampling rate was $f_{\mathrm{sample}} = 500$ kHz and the anti-aliasing filter cutoff was $f_{\mathrm{cut\text{-}off}} = 150$ kHz. To generate AM signals, V_{sd1} and V_{sd2} were driven at carrier frequencies f_{c1} and f_{c2}, respectively. Recorded modulated output signals were demodulated digitally in MATLAB.

C. Liquid-Gated Active Electrode Measurement Results

1) Two-channel pulse-based measurements: For the data shown in Fig. 4, two test signals mimicking action potentials from two individual neurons were applied to the two liquid gates. Each test signal consisted of a series of 2 mV Gaussian pulses with full-width at half-maximum (FWHM) of 2.2 ms and 20 ms spacing between pulses. The pulse trains applied to gate 1 and gate 2 were offset by 10 ms so that crosstalk between channels, if non-negligible, would be easily observed. The dc offsets of gate 1 and gate 2 were set to -120 mV ($\sim$

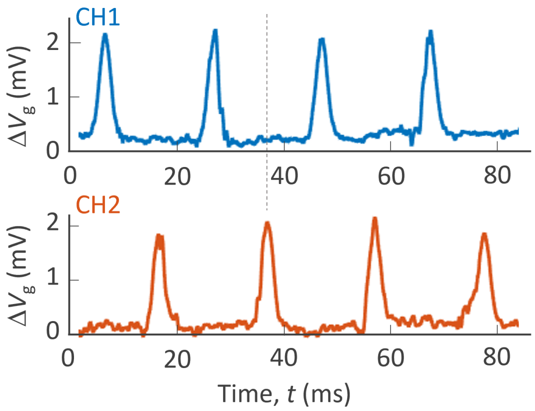

Fig. 4. Reconstructed signals from multiplexed operation of two GFETs. Amplitude-modulated currents were produced in each channel, with f_{c1} = 81 kHz and f_{c2} = 91 kHz. FWHM of the Gaussian peaks is 2.2 ms.

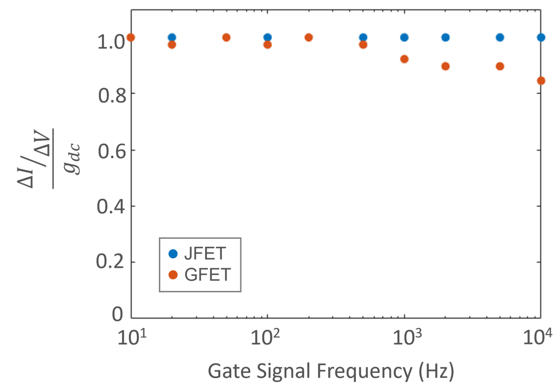

Fig. 5. Dynamic transconductance of a GFET sensor. The amplitude modulation of the current, ΔI, was measured when a sinusoidal signal of amplitude ΔV was applied to the liquid gate. The ratio $\Delta I/\Delta V$ is normalized by the dc transconductance, g_{dc}. The experiment used a carrier frequency f_c = 79 kHz.

-100 mV from the Dirac point) to maximize transconductance, dI/dV_g. The sensors were operated in multiplexed AM mode (Fig. 1), with carrier frequencies f_{c1} = 81 kHz and f_{c2} = 91 kHz. The amplitudes of the reconstructed signals were 1.9±0.1 mV for CH1, and 1.7±0.1 mV for CH2, and the noise in the reconstructed signal (Fig. 4) is 100 μV_{rms} for CH1 and 110 μV_{rms} for CH2 for a 1 kHz bandwidth. The baseline noise is intrinsic to the device (not introduced by multiplexing) and could be lowered with improved fabrication [11]. There is no observable crosstalk between the two channels. We also tested spike patterns that overlapped in time. We reduced the offset between the gate-1 pulse train and the gate-2 pulse train from 10 ms to 0.8 ms. The SNR was unchanged and no crosstalk was observed. Overall, Fig. 4 demonstrates that single-neuron action-potentials with frequency components ∼1 kHz could be multiplexed and recorded using this approach.

Our system for sending independent signals to each graphene sensor differs from the previously published methods to test crosstalk in a multiplexed graphene-based neurosensor array. In [8], for example, the authors used polyelectrolyte droplets that were inkjet-printed onto graphene sensors. However, the graphene sensor response to the polyelectrolyte gate was different than its response to a standard liquid electrolyte gate. In comparison, our dual-liquid gate technique offers a simple approach for testing crosstalk and more closely emulates the graphene-to-liquid interface that occurs *in-vivo*.

2) Bandwidth analysis for graphene neurosensors: To quantify the sensing bandwidth of our system, we measured the dynamic transconductance of a GFET sensor. We used AM with a carrier frequency of 79 kHz and applied a pure-tone sinusoidal voltage signal to the gate, ΔV. The frequency of ΔV was varied from 10 Hz to 10 kHz. When a 10 Hz voltage signal was applied to the gate, the amplitude of the current modulation, ΔI, was equal to $g_{dc} \cdot \Delta V$, where g_{dc} is the dc transconductance (Fig. 3). When a 10 kHz voltage signal was applied, however, ΔI was slightly less than $g_{dc} \cdot \Delta V$. To describe this frequency-dependent effect, we define the dynamic transconductance, g_{ac}, such that $\Delta I = g_{ac}\Delta V$. Fig. 5 shows the ratio of g_{ac}/g_{dc} as the signal frequency is increased. For comparison, the same experiment was performed using a commercially available junction field-effect transistor (JFET) (InterFET 2N4339). The JFET was chosen because it has similar resistance and transconductance as the graphene FET at comparable bias levels.

Figure 5 shows a significantly better sensor bandwidth than previous reports of GFET-based active electrodes. Previous work found $g_{ac}/g_{dc} = 0.5$ at 1 kHz, and $g_{ac}/g_{dc} = 0.25$ at 10 kHz [8]. To explain this improved response to higher frequency signals, consider the parasitic capacitance between the liquid gate and the SU-8-coated metal electrodes. When an ac voltage is applied to the liquid gate, there is some current flow through the parasitic capacitance. Thus, the higher frequency test signals are attenuated before reaching the graphene sensor. In our design, the parasitic capacitance is decreased by minimizing the overlap area between the metal electrodes and the liquid gate (the overlap area in our device is ∼ 0.03 mm^2). If the voltage signals were generated by neurons, the effective parasitic capacitance would be even less because the local voltage change generated by a neuron only extends ∼100 μm from the neuron. We conclude that the small parasitic capacitance of our device geometry more closely approximates the small parasitic capacitance associated with *in-vivo* measurements of single neurons. Therefore, near-unity g_{ac}/g_{dc} can be expected for single-neuron recordings in the kilohertz range.

3) Carrier frequency analysis for graphene neurosensors: To further evaluate the graphene-based FDM sensors, we investigated constraints on carrier frequency. The maximum carrier frequency, f_{max}, affects the number of frequency channels that can share a single output wire. At high carrier frequencies, current flows from the graphene sensor into the liquid electrolyte via capacitive coupling between the graphene and the liquid. Based on [21], we define a threshold frequency, f_{th}, at which the graphene-to-liquid current is equal to the current flowing through the graphene channel. The threshold frequency is given by $f_{th} = (2\pi RC)^{-1}$ where R is the resistance of the graphene channel and C is the capacitance

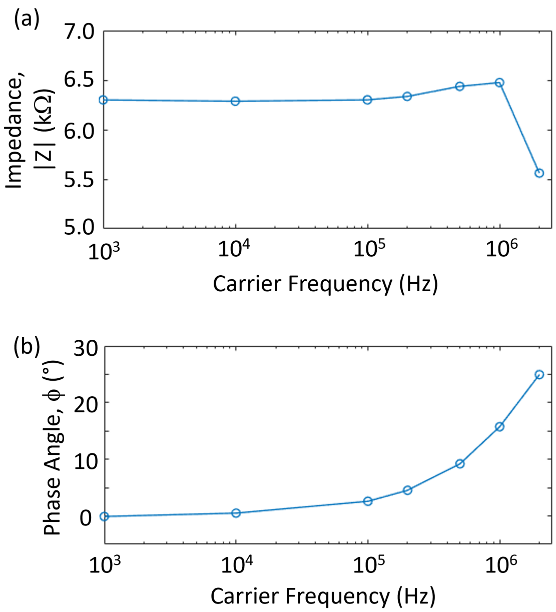

Fig. 6. Measured impedance of GFET for different carrier frequencies. (a) Magnitude of GFET impedance as a function of frequency. The impedance changes by less than 10% up to 1 MHz. (b) Phase difference between the applied source-drain bias and the measured current. The phase difference reaches about 15° at f_c = 1 MHz.

between the graphene channel and the liquid. The quantum capacitance of graphene sets an upper limit for C [22], [23], and R can be expressed in terms in terms of carrier scattering time, τ, therefore we find $f_{\text{th}} > (\tau v_F^2)/(4\pi L^2)$ where $v_F \approx 10^6$ m/s is the Fermi velocity, and L is the channel length. Interestingly, this lower bound is independent of channel width, independent of V_G, and independent of electrolyte composition (note that $4\pi L^2/\tau v_F^2$ corresponds to the carrier diffusion time for a length of order L). Previous work on electrolyte gated graphene showed $\tau \sim$70 fs [24], suggesting that $f_{\text{th}} > 2.2$ MHz when $L = 50\,\mu$m. These theoretical considerations also suggest the possibility of operating liquid-gated GFETs at even higher carrier frequencies when $L < 50\,\mu$m.

We tested our graphene FET sensors with carrier frequencies up to 2 MHz, as shown in Fig. 6. Previous authors have performed similar testing, but at lower frequencies (below 500 kHz) [8], [21]. The drain current, I, was monitored using a high-bandwidth current amplifier. The ac bias voltage, V, had an rms amplitude of 0.1 V. The complex-valued impedance, $Z = V/I$, is shown in Fig. 6. The phase of the impedance is zero at low frequency, demonstrating purely resistive behavior. As the frequency increases to 1 MHz, the magnitude of the impedance $|Z|$ is stable (changes by less than 10%) and the phase reaches 15°. Fig. 6 confirms that carrier frequencies up to at least 1 MHz can be used to multiplex signals from GFET sensors (i.e. at 1 MHz most of the current stays in the graphene channel and is still modulated by changes in the graphene resistance). This has important consequences for scalability of the FDM system, as described below.

D. Future Graphene Neurosensor Arrays

To realize graphene-based FDM multiplexing with reduced wire count, a row and column geometry is required. Each column of GFETs would receive the same carrier frequency, while each row of GFETs would be connected to a common output wire. The signal from each GFET can be uniquely identified by its row number and carrier frequency, so spatial resolution is maintained. Prior work has demonstrated the feasibility of fabricating such row/column arrays [8].

The set of carrier frequencies should be chosen from the range $f_{\text{max}}/2$ to f_{max} so that harmonics produced by the lower frequencies do not interfere with the higher frequency bands. With carrier frequencies spaced by 10 kHz, it would be possible to fit 50 frequency division slots in the range of 500 kHz to 1 MHz. For a square array, 50 columns and 50 rows, a total of 2,500 sensors could be operated with 100 wires using this approach. If more rows were added to the array, each additional output wire would enable recordings from 50 additional sensors.

We note that while the fused silica used in our fabricated prototype is rigid, this can be replaced by a flexible substrate such as polyimide to make a flexible version of the same structure for implantable devices [8]. Based on previous work with polyimide, we do not expect the electrical characteristics to be meaningfully affected by the choice of substrate. Additionally, previous work has demonstrated that the graphene channel dimensions can be shrunk for higher spatial resolution ($W = L = 20\,\mu$m) and still detect single neuron firing events with sufficient SNR (effective gate noise $< 30\,\mu$V) [11].

III. Conclusion

In this work, we evaluated GFET devices for their use as FDM-based active electrodes for neurosensor readout, for which we introduced a new testing platform based on dual-liquid gates that enables independent actuation, mimicking individual neurons. Using a fabricated 2-channel GFET prototype, we demonstrated multiplexed detection with no observable crosstalk using signals in the kilohertz band. We observed minimal performance degradation for signals up to 10 kHz, demonstrating that multiplexed GFETs are capable of single neuron recordings. We also showed that our liquid-gated graphene devices retain their resistive behavior when using carrier frequencies up to 1 MHz, demonstrating sufficient space in the frequency domain to scale such a GFET-based FDM system to much larger sensor arrays. While further work is required to fabricate and characterize large arrays of GFET FDM sensors, the characteristics of our test devices suggest that a reasonable target is 2,500 sensors operated with only 100 access wires using this approach.

Acknowledgment

This work was supported in part by the National Institutes of Health under Award R21EY030007. Part of this research was conducted at the Northwest Nanotechnology Infrastructure site at Oregon State University (NNCI-2025489).

REFERENCES

[1] G. Hong and C. M. Lieber, "Novel electrode technologies for neural recordings," *Nature Reviews Neuroscience*, vol. 20, no. 6, pp. 330–345, 2019.

[2] R. Garcia-Cortadella, G. Schwesig, C. Jeschke, X. Illa, A. L. Gray, S. Savage, E. Stamatidou, I. Schiessl, E. Masvidal-Codina, K. Kostarelos *et al.*, "Graphene active sensor arrays for long-term and wireless mapping of wide frequency band epicortical brain activity," *Nature Communications*, vol. 12, no. 1, pp. 1–17, 2021.

[3] B. C. Raducanu, R. F. Yazicioglu, C. M. Lopez, M. Ballini, J. Putzeys, S. Wang, A. Andrei, V. Rochus, M. Welkenhuysen, N. v. Helleputte *et al.*, "Time multiplexed active neural probe with 1356 parallel recording sites," *Sensors*, vol. 17, no. 10, p. 2388, 2017.

[4] R. Chen, A. Canales, and P. Anikeeva, "Neural recording and modulation technologies," *Nature Reviews Materials*, vol. 2, no. 2, pp. 1–16, 2017.

[5] R. Biran, D. C. Martin, and P. A. Tresco, "Neuronal cell loss accompanies the brain tissue response to chronically implanted silicon microelectrode arrays," *Experimental Neurology*, vol. 195, no. 1, pp. 115–126, 2005.

[6] J. W. Salatino, K. A. Ludwig, T. D. Kozai, and E. K. Purcell, "Glial responses to implanted electrodes in the brain," *Nature Biomedical Engineering*, vol. 1, no. 11, pp. 862–877, 2017.

[7] N. Schaefer, R. Garcia-Cortadella, J. Martínez-Aguilar, G. Schwesig, X. Illa, A. M. Lara, S. Santiago, C. Hébert, G. Guirado, R. Villa *et al.*, "Multiplexed neural sensor array of graphene solution-gated field-effect transistors," *2D Materials*, vol. 7, no. 2, p. 025046, 2020.

[8] R. Garcia-Cortadella, N. Schafer, J. Cisneros-Fernandez, L. Ré, X. Illa, G. Schwesig, A. Moya, S. Santiago, G. Guirado, R. Villa *et al.*, "Switchless multiplexing of graphene active sensor arrays for brain mapping," *Nano Letters*, vol. 20, no. 5, pp. 3528–3537, 2020.

[9] J. Kim, C. V. Fengel, S. Yu, E. D. Minot, and M. L. Johnston, "Frequency-division multiplexing with graphene active electrodes for neurosensor applications," *IEEE Transactions on Circuits and Systems II: Express Briefs*, vol. 68, no. 5, pp. 1735–1739, 2021.

[10] J. J. Jun, N. A. Steinmetz, J. H. Siegle, D. J. Denman, M. Bauza, B. Barbarits, A. K. Lee, C. A. Anastassiou, A. Andrei, Ç. Aydın *et al.*, "Fully integrated silicon probes for high-density recording of neural activity," *Nature*, vol. 551, no. 7679, pp. 232–236, 2017.

[11] N. Schaefer, R. Garcia-Cortadella, A. B. Calia, N. Mavredakis, X. Illa, E. Masvidal-Codina, J. de la Cruz, E. Del Corro, L. Rodríguez, E. Prats-Alfonso *et al.*, "Improved metal-graphene contacts for low-noise, high-density microtransistor arrays for neural sensing," *Carbon*, vol. 161, pp. 647–655, 2020.

[12] M. K. Blees, A. W. Barnard, P. A. Rose, S. P. Roberts, K. L. McGill, P. Y. Huang, A. R. Ruyack, J. W. Kevek, B. Kobrin, D. A. Muller *et al.*, "Graphene kirigami," *Nature*, vol. 524, no. 7564, pp. 204–207, 2015.

[13] C. Lee, X. Wei, J. W. Kysar, and J. Hone, "Measurement of the elastic properties and intrinsic strength of monolayer graphene," *Science*, vol. 321, no. 5887, pp. 385–388, 2008.

[14] S. K. Rastogi, G. Raghavan, G. Yang, and T. Cohen-Karni, "Effect of graphene on nonneuronal and neuronal cell viability and stress," *Nano Letters*, vol. 17, no. 5, pp. 3297–3301, 2017.

[15] W. C. Lee, C. H. Y. Lim, H. Shi, L. A. Tang, Y. Wang, C. T. Lim, and K. P. Loh, "Origin of enhanced stem cell growth and differentiation on graphene and graphene oxide," *ACS Nano*, vol. 5, no. 9, pp. 7334–7341, 2011.

[16] F. Veliev, A. Briançon-Marjollet, V. Bouchiat, and C. Delacour, "Impact of crystalline quality on neuronal affinity of pristine graphene," *Biomaterials*, vol. 86, pp. 33–41, 2016.

[17] A. Bendali, L. H. Hess, M. Seifert, V. Forster, A.-F. Stephan, J. A. Garrido, and S. Picaud, "Purified neurons can survive on peptide-free graphene layers," *Advanced Healthcare Materials*, vol. 2, no. 7, pp. 929–933, 2013.

[18] S. K. Rastogi, J. Bliley, D. J. Shiwarski, G. Raghavan, A. W. Feinberg, and T. Cohen-Karni, "Graphene microelectrode arrays for electrical and optical measurements of human stem cell-derived cardiomyocytes," *Cellular and Molecular Bioengineering*, vol. 11, no. 5, pp. 407–418, 2018.

[19] Y. Lu, X. Liu, R. Hattori, C. Ren, X. Zhang, T. Komiyama, and D. Kuzum, "Ultralow impedance graphene microelectrodes with high optical transparency for simultaneous deep two-photon imaging in transgenic mice," *Advanced Functional Materials*, vol. 28, no. 31, p. 1800002, 2018.

[20] M. A. Brown, L. Barker, L. Semprini, and E. D. Minot, "Graphene biotransistor interfaced with a nitrifying biofilm," *Environmental Science and Technology Letters*, vol. 2, no. 4, pp. 118–122, 2015.

[21] S. Drieschner, A. Guimerà, R. G. Cortadella, D. Viana, E. Makrygiannis, B. M. Blaschke, J. Vieten, and J. A. Garrido, "Frequency response of electrolyte-gated graphene electrodes and transistors," *Journal of Physics D: Applied Physics*, vol. 50, no. 9, p. 095304, 2017.

[22] H. Xu, Z. Zhang, and L.-M. Peng, "Measurements and microscopic model of quantum capacitance in graphene," *Applied Physics Letters*, vol. 98, no. 13, p. 133122, 2011.

[23] J. Xia, F. Chen, J. Li, and N. Tao, "Measurement of the quantum capacitance of graphene," *Nature Nanotechnology*, vol. 4, no. 8, pp. 505–509, 2009.

[24] M. A. Brown, M. S. Crosser, M. R. Leyden, Y. Qi, and E. D. Minot, "Measurement of high carrier mobility in graphene in an aqueous electrolyte environment," *Applied Physics Letters*, vol. 109, no. 9, p. 093104, 2016.